RESEARCH PAPER

A New Approach for Measuring Viscoelastic Properties of Soft Materials Using the Dynamic Response of a Spherical Object Placed at the Sample Interface

H. Koruk[1,2] · H. O. Koc[1] · S. B. Yurdaer[1] · A. Besli[1] · A. N. Pouliopoulos[2]

Abstract

Background There are several techniques to characterize the mechanical properties of soft materials, such as the indentation method and the method based on the application of a spherical object placed inside the sample. The indentation systems usually yield the elastic properties of materials and their mathematical models do not consider the inertia of the sample involved in motion and radiation damping, while placing an object inside the sample is not practical and this procedure can alter the mechanical properties of the sample for the method based on the application of a bubble/sphere placed inside the sample.

Objective A new approach for the identification of the viscoelastic properties of soft materials using the dynamic response of a spherical object placed at the sample interface was proposed.

Methods The spherical object placed at the sample interface was pressed using an electromagnet and the dynamic response of the spherical object was tracked using a high-speed camera, while the dynamic response of the spherical object placed at the sample interface was estimated using a comprehensive analytical model. The effects of the shear modulus, viscosity, Poisson's ratio and density of the soft sample, the radius and density of the spherical object and the damping due to radiation were considered in this mathematical model. The shear modulus and viscosity of the soft sample were determined by matching the experimentally identified and theoretically estimated responses of the spherical object.

Results The shear moduli and viscosities of the three phantoms with the gelatin mass ratios of 0.20, 0.25 and 0.29 were measured to be 3450, 4300 and 4950 Pa and 12.5, 14.0 and 15.0 Pa·s, respectively. The shear modulus and viscosity of the phantom increases as the gelatin mass ratio increases. The frequency of oscillations of the hemisphere placed at the phantom interface increases as the gelatin mass ratio increases due to stiffness increase.

Conclusions After matching the experimental and theoretical steady-state displacements and amplitudes of oscillations of the hemisphere at the sample interface, the comparison of the experimentally identified and theoretically predicted frequency of oscillations further confirmed the identified material properties of the samples. The approach presented here is expected to provide valuable information on material properties in biomedical and industrial applications.

Keywords Soft material · Shear modulus · Viscosity · Viscoelastic properties · Spherical object · Sample interface

Introduction

Viscoelastic materials such as tissue, tissue-mimicking materials and gels exhibit both viscous and elastic characteristics when exposed to a dynamic force, and the viscoelastic properties of soft materials are needed in many applications [1–5]. The indentation method [6–11], rheometry/viscometry [12–14] and atomic force microscopy [15–17] are often used for the assessment of the mechanical properties of soft materials. In addition, the method based on the application of a bubble or sphere placed inside the soft material or a bubble placed at the interface of the soft sample has been used for the evaluation of soft materials in recent years [18–20]. Among these methods, the indentation method is quite common for the characterization of the mechanical properties of soft materials. However, the traditional indentation systems can be quite complicated [21], they usually yield only the determination of the elastic properties of

✉ H. Koruk
korukh@mef.edu.tr; hasan.koruk@kcl.ac.uk

1 Faculty of Engineering, MEF University, Istanbul 34396, Turkey

2 Department of Surgical & Interventional Engineering, School of Biomedical Engineering & Imaging Sciences, King's College London, London, UK

materials [22–25], and the mathematical models used for the indentation tests do not consider the inertia of the soft material involved in motion and the damping due to radiation [24, 26]. For the method based on the application of a spherical object placed inside the soft material [18–20], placing or creating an object inside the soft material is not practical and this procedure can alter the mechanical properties of the soft material.

There is a big number of studies for the identification of viscoelastic properties of soft materials using rheometry/viscometry, indentation method, and atomic force microscopy (AFM). Dakhil et al. [12] determined the storage and loss moduli of cells using a rheometer and Peng et al. [13] identified the dilute solution viscosities of some cellulose nanocrystal dispersions by using a capillary viscometer. A spherical object at the sample interface is forced in indentation methods and AFM. For example, Nayar et al. [7] determined the storage and loss moduli of some samples of agar (being a representative material for biological tissues) and Boyer et al. [21] evaluated the stiffness and damping of skin via the dynamic indentation method. Chim et al. [2] measured the viscoelastic properties of living cells and Darling et al. [27] determined the elastic and viscoelastic properties of porcine chondrocytes using AFM.

Some advanced mathematical models for the dynamic response of a sphere placed at the interface of the sample have been proposed in recent years [28–31]. An advanced analytical model for the dynamic response of a sphere placed at the elastic material (without damping) interface was proposed in 2021 [30] and this model was used to identify the elastic properties of some soft materials in 2022 [32, 33]. In addition, by exploiting an equivalent viscous damping ratio for the soft sample in the analytical model for an elastic medium (without damping) in [30], the equivalent viscous damping ratios of some soft materials were identified [32, 33]. However, this approach produces an equivalent viscous damping ratio for the system (i.e., for the system consisting of a sphere placed at the sample interface), and the exact damping of the soft sample could not be identified. Therefore, first, different mathematical models for the static response of a sphere placed at the sample interface were evaluated and an improved mathematical model for the static response of a sphere placed at the sample interface was proposed [31]. Then, a comprehensive mathematical model for the dynamic response of a sphere placed at the viscoelastic material interface was developed [31]. In addition to the shear modulus of the sample and the radius of the spherical object, this mathematical model takes into account the density, Poisson's ratio and viscosity of the sample, the mass of the spherical and the damping due to radiation, and the model can be used for both small and large deformations of the sample [31]. This model is believed to be the most comprehensive model for the dynamic response of a spherical

object placed at the interface of the sample. However, this model proposed in 2022 has not been used in any applications yet. Therefore, a new approach for the characterization of the viscoelastic properties of soft materials based on this model was proposed in this current study.

Gelatin phantoms are widely used as tissue mimicking materials in practice [14, 34–37]. Therefore, several soft samples prepared using gelatin powder and boiling water were used in this study. The spherical object placed at the sample interface was pressed using an electromagnet and the dynamic response of the spherical object was tracked using a high-speed camera. The displacement of the spherical object as a function of time was determined by processing the captured video. The dynamic response of the spherical object placed at the sample interface was estimated using the aforementioned comprehensive mathematical model, after revising the mathematical model for a trapezoidal pulsed force. Overall, the shear modulus and viscosity of the soft sample were determined by matching the experimentally identified and theoretically predicted responses of the spherical object. The results showed that the period of oscillations of the hemisphere placed at the phantom interface decreases (or its frequency of oscillations increases) and the shear modulus and viscosity of the phantom increase with the increasing gelatin mass ratio, as expected. Thanks to the simple experimental system and the comprehensive mathematical model that takes into account different system parameters including the shear modulus, density and viscosity of the soft sample, the mass and radius of the spherical object and the damping due to radiation, the approach used in this study can be exploited to determine the viscoelastic properties of soft materials in biomedical and industrial applications, such as optimization of process conditions and determination of end-product requirements of materials.

Procedure

Mathematical Model

In addition to the shear modulus of the sample and the radius of the sphere, the effects of the density and viscosity of the sample, the mass of the sphere and the damping due to radiation on the response of a spherical object placed at the sample interface can be significant when the loading is dynamic. Therefore, the mathematical model that takes into account the shear modulus, viscosity, Poisson's ratio and density of the soft sample, the radius and density of the sphere and the radiation damping proposed by Koruk in 2022 [31] was used to predict the dynamic response of the spherical object placed at the sample interface (Fig. 1) in this study. This model is based on the Kelvin-Voigt model and it was shown to be valid for both small ($u << R$) and large (u

Fig. 1 The schematic picture for a sphere placed at the sample interface
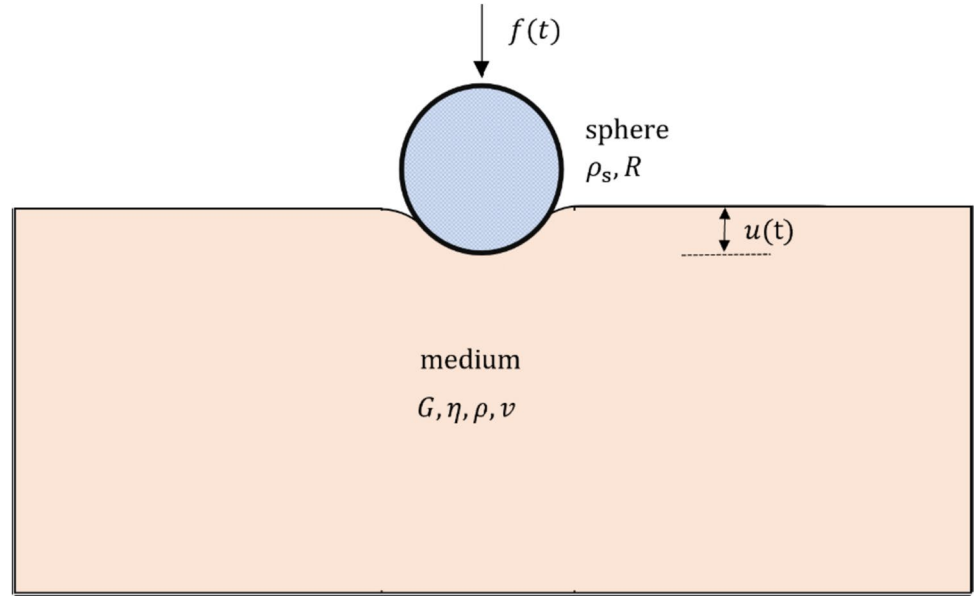
> $R/5$) deformations of the sample [31]. It should be noted that the Kelvin-Voigt model is widely used in the literature to simulate soft materials, such as gelatin phantoms [1, 18, 20, 38–40]. The model was formulated for a rectangular pulse with an amplitude of f_0 and a duration of τ shown in Fig. 2(a) in [31]. Hence, the time-domain response of the spherical object placed at a viscoelastic material interface exposed to a rectangular pulse can be estimated using [31]:

$u_0 = \left(\frac{3f_0}{4E^* \sqrt{R}} \right)^{2/3}$ is the static displacement of the spherical object. Here, E^* represents the reduced Young's modulus predicted as $1/E^* = \left(1 - v_{\text{sphere}}^2 \right)/E_{\text{sphere}} + \left(1 - v^2 \right)/E$ where E_{sphere} and v_{sphere} are the Young's modulus and Poison's ratio of the sphere material, respectively. It is worth remembering that the reduced Young's modulus becomes $\widetilde{E}^* = 2(G - j\omega\eta)(1 + v)/\left(1 - v^2\right)$ for a homogeneous iso-

$$u(t) = \frac{1}{2\pi} \int_{-\infty}^{\infty} \frac{\left\{ 1 + 0.5\left[1 - (v - 0.35)\frac{u_0}{R} \right] \right\} F(\omega)e^{-j\omega t}}{\frac{1}{3}\pi R^3 \left(4\rho_s + \frac{u_0}{R}\rho \right)(-\omega^2) + \left[\frac{1}{2}\left(\beta + \frac{u_0}{R} \right)\left(\sqrt{\frac{\rho}{G - j\omega\eta}}R \right)(-j\omega) + 1 \right]\left[1 - (v - 0.35)\frac{u_0}{R} \right]1.5f_0^{1/3}\left(\frac{4\widetilde{E}^* \sqrt{R}}{3} \right)^{2/3}} \, d\omega \tag{1}$$

where $u(t)$ shows the displacement of the sphere at any time t, and $F(\omega)$ is the Fourier transform of the rectangular pulse given by:

$$F(\omega) = -\frac{jf_0}{\omega}\left(e^{j\omega\tau} - 1 \right) \tag{2}$$

Here, G, ρ, η and v are the shear modulus, density, viscosity and Poisson's ratio of the sample, R and ρ_s are the radius and density of the spherical object, respectively, $\beta = 0.5$, $j = \sqrt{-1}$, and shows the angular frequency. It should be noted that

tropic sample and a rigid spherical object. Interested readers may refer to [31] for the derivation and other details of the mathematical model. Due to the magnetic force created using an electromagnet and a small magnet fixed to the spherical object placed at the sample interface, it is difficult to stabilize the spherical object and prevent its unwanted rotations. Therefore, a hemisphere was used in this study. It should be noted that, as long as the correct density and radius of the spherical object are used in the mathematical model, a hemisphere can be used in the mathematical model proposed in [31].

Fig. 2 Rectangular (**a**) and trapezoidal (**b**) pulsed force
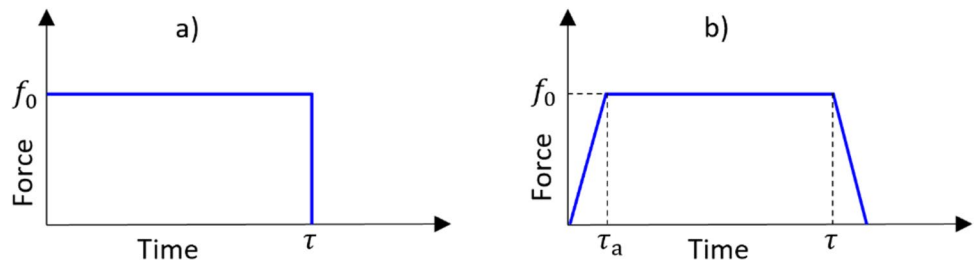
It is worth noting that the nonlinear relationship between the force and displacement was linearized around the steady-state displacement using the Taylor's expansion in this mathematical model. This approach was evaluated and validated (e.g., using finite element models) in the literature [30, 31, 41]. This model produces an approximate solution for a dynamic Hertz model. The mathematical model was explained in Appendix A. Readers may refer to references [30, 31, 41] for further details about the mathematical modelling of a spherical object located at the interface of elastic and viscoelastic media.

In practice, obtaining an ideal rectangular pulse shown in Fig. 2(a) is not possible. The temporal evolution of the magnetic force is described by a trapezoidal pulse with a finite ramp or rise time (τ_a) as shown in Fig. 2(b) [18]. It is known that, although the steady-state displacement remains the same, the amplitudes of oscillations (especially the amplitude of the first peak) decrease as the rise time increases [42–44]. The Fourier transform of a trapezoidal pulsed force shown in Fig. 2(b) is given by [18]:

$$F(\omega) = -\frac{f_0}{\tau_a \omega^2} \left(e^{j\omega\tau} - 1 \right) \left(e^{j\omega\tau_a} - 1 \right) \tag{3}$$

Therefore, we updated the mathematical model for a trapezoidal pulsed force here, by substituting the expression of $F(\omega)$ given in equation (3) in equation (1).

Experimental Setup

A hemisphere (with a radius R) placed at the interface of the sample (with a uniform shear modulus G, density ρ, viscosity η and Poisson's ratio v) was pressed using a magnetic force (f) and the displacement of the hemisphere $u(t)$ was tracked using a high-speed camera. The schematic picture for the experimental setup and the picture of the hemisphere placed at the phantom surface are shown in Fig. 3. A small cylindrical magnet (radius: 12.3 mm and thickness: 5 mm) was fixed (glued) to the top surface of the hemisphere to be able to apply a force by an electromagnet (KK-P50/30 DC12V, Yueqing Kaka Electric Co. Ltd., China) to the hemisphere placed at the sample interface. A power supply (GPS-3303, GW Instek, Taiwan) was used to run the electromagnet in the experiments. The electromagnet was fixed to the frame using the electromagnet holder. The hemisphere holder was used to prevent the unwanted rotation of the hemisphere. The hemisphere holder was a thin-walled cylinder with an inner radius of around 24.8 mm, and the diameter of the magnet was 24.6 mm. The magnet fixed to the hemisphere could easily slide through the thin-walled cylinder. The videos were captured at 240 fps and the resolution was around 0.06 mm/pixel. The displacement of the hemisphere from the videos as a function of time (t) was tracked using the Matlab software (MathWorks, Natick, MA, USA). The sensitivity of the load cell used to measure the force amplitude was 0.1 mN.

The hemisphere, hemisphere holder and electromagnet holder were designed using the SolidWorks software (Dassault Systemes SolidWorks Corporation, Chicago, IL, USA) and these components were manufactured using a 3D printer (Ultimaker 2 Extended+, Utrecht, Netherlands) and PLA filaments. The layer resolution for the 3D printing was 0.06 mm. After the hemisphere was manufactured, it was grinded for further smoothening. The radius and mass of

Fig. 3 The schematic picture for the experimental setup and the picture of the hemisphere placed at the phantom surface (the radius of the hemisphere was 12.15 mm, and the height, width and length of the phantom were 30, 100 and 170 mm)
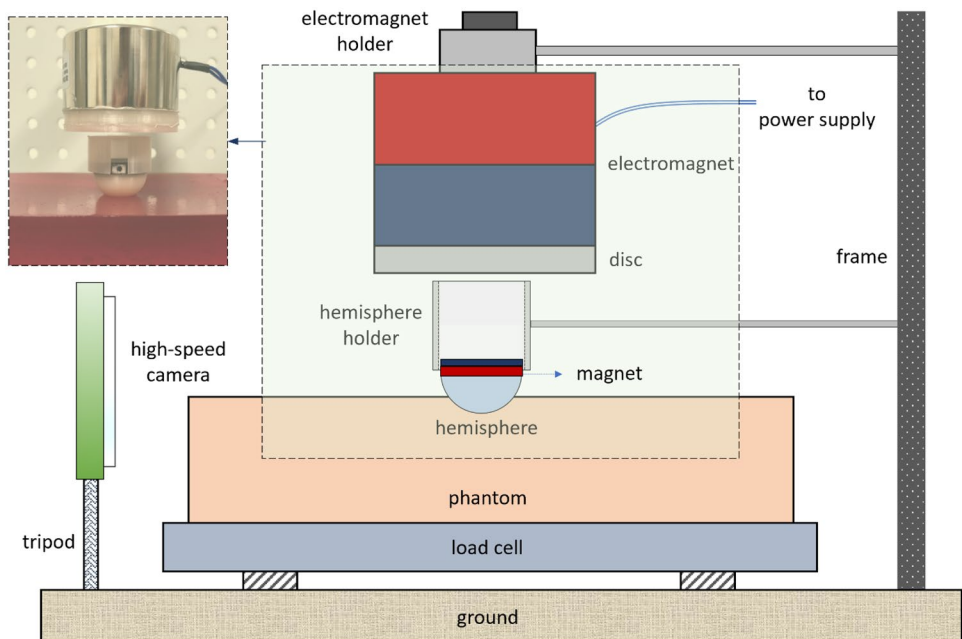
the hemisphere was 12.15 mm and 4.11 g, respectively. The mass of the magnet was 10.92 g. The equivalent density of the spherical object was calculated to be 2000.5 kg/m^3. Hence, the inertial effects of the hemisphere and magnet were taken into account. It should be noted that the inertial effects of the spherical object and the mass of the medium involved in motion were investigated in detail in [31]. As the gelatin phantoms are widely used as tissue mimicking materials in practice, we prepared soft samples using gelatin powder and boiling water. It should be noted that phantoms with different mechanical and physical components can be prepared by controlling the amount of components in the phantom and duration for cooling and leaving to set at working temperature [45]. In this current study, after the solution of the gelatin and water was prepared, it was stored in the refrigerator (4 °C) for 240 minutes and then it was left to set at room temperature (25 °C) for 30 minutes before the experiments. Here, three different gelatin phantoms with different viscoelastic properties were prepared by using different amount of gelatin powder. The properties of the three phantoms are listed in Table 1. The dimensions of the phantoms were around 30 mm × 100 mm × 170 mm. The densities of the soft samples were computed by using their measured masses and dimensions. The phantom with a gelatin mass ratio of 0.25 was tested for three different force levels (i.e., for 240.2, 270.2, and 291.5 mN) to explore the effect of loading.

The experiments were performed as follows. The test sample was placed on the load cell and the hemisphere (fixed to the magnet) was inserted inside the hemisphere holder. The electromagnet and the high-speed camera were activated at the same time. Once the electromagnet was activated, it applied a force to the hemisphere, and the hemisphere started to deform the gelatin phantom. The electromagnet applied a force to the hemisphere for a duration of τ. The duration was $\tau = 0.4$ s in this study. The rise time for the electronic circuit in this study was around $\tau_a = 50$ ms. The sample normalized force (i.e., the force divided by the maximum force) measurements for the electromagnet in this study presented in Fig. 4 showed that the rise time was $\tau_a = 47.3 \pm 0.5$ ms. It should be noted that three experiments were repeated for each test case to calculate the average as well as the standard

deviations (e.g., Figs. 6, 7, 8). The frames from a sample captured video at the beginning (the left panel), the maximum deformation (the middle panel) and the steady-state position (the right panel) for the hemisphere placed at the interface of a gelatin phantom are shown in Fig. 5. Here, a piece of paper with a black marker was glued on the magnet to be used as the template for accurate tracking the motion of the hemisphere via image processing.

Extraction of Viscoelastic Properties

The theoretical response of the spherical object placed at the sample interface was determined by solving equation (1); noting that the expression for a trapezoidal pulse given in equation (3) was used in the calculations. For this purpose, the excitation duration τ was discretized with N (e.g., 500) points and the calculations were repeated at all points using the Matlab software (Mathworks, Natick, MA). The captured video was processed to find the experimental dynamic response of the spherical object. For this purpose, a template (see the left panel in Fig. 5) was determined and the MATLAB *normxcorr2* function was used to track the motion of the spherical object. The Poisson's ratio of the soft samples was assumed to be 0.45 in this study, as it is done in practice [6, 46, 47]. It should be noted that there is no effect of the viscosity of the sample on the steady-state displacement of the hemisphere located at the phantom interface. (a) Therefore, the shear modulus of the sample was determined as following. i) Using an initial value for the shear modulus of the material (e.g., $G = 2$ Pa) in the analytical model, the response of the hemisphere was predicted and the difference between the experimental and predicted steady-state displacements was calculated. ii) Using a higher value for the shear modulus of the material (e.g., $G = 4$ Pa) in the analytical model, the response of the hemisphere was calculated and the difference between the experimental and predicted steady-state displacements was
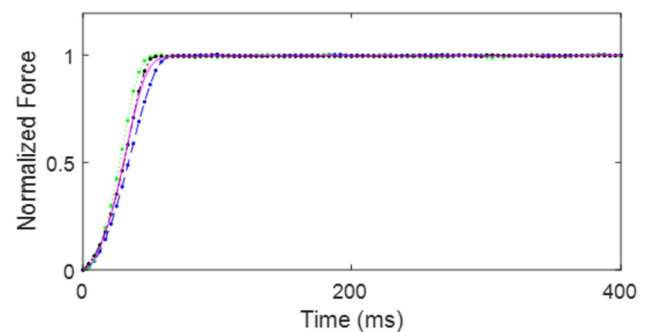
Table 1 The properties of the three phantoms (the height, width and length of the phantom were 30, 100 and 170 mm)

Phantom	Gelatin Mass Ratio	Phantom Density (kg/m^3)
Sample 1	0.20	1043.8
Sample 2	0.25	1084.2
Sample 3	0.29	1099.7

Fig. 4 The sample normalized force (i.e., the force divided by the maximum force) measurements for the electromagnet

Fig 5 The frames from a sample captured video at the beginning (the left panel), the maximum deformation (the middle panel) and the steady-state position (the right panel) for the hemisphere placed at the interface of a gelatin phantom
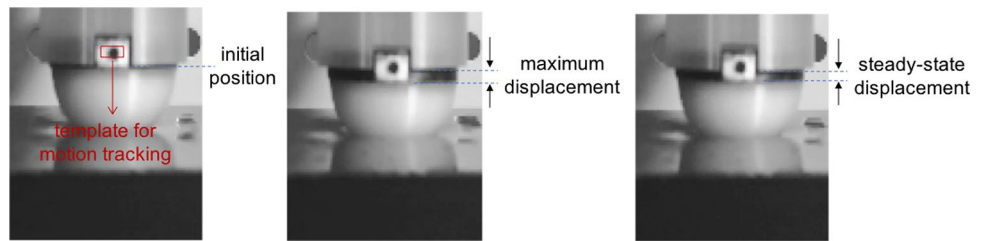
determined. iii) The calculations in the previous step were repeated for different (higher) values of the shear modulus of the sample (e.g., $G = 8, 16, 32, \ldots, 9600$ Pa). The error reached a minimum value at a specific value of the shear modulus (e.g., $G = 4096$ Pa) and then it increased. iv) Based on the minimum value of the error, a narrower range for the shear modulus (e.g., $G = 2000 - 9000$ Pa) was determined. v) The calculations in the previous step were repeated by changing the value of the shear modulus (e.g., $G = 2050, 2100, \ldots, 9000$ Pa) in the analytical model to refine the estimate of the shear modulus. vi) The value of the shear modulus producing the minimum error was determined to be the shear modulus of the sample. The identified value of the shear modulus of the sample matched the experimental and theoretical steady-state displacements. (b) Next, by comparing the experimental and theoretical amplitudes of oscillations, the viscosity of the sample was determined. Overall, the viscosity of the sample was determined by minimizing the error between the experimentally identified amplitudes of oscillations and the amplitudes of oscillations predicted by varying the value of the viscosity of the material in the analytical model, using least-squares fitting. (c) The comparison of the experimentally identified and theoretically predicted frequency of oscillations would further confirm the identified material properties of the sample.

Results and Discussion

The average of the experimentally identified responses of the hemisphere placed at the phantom interfaces with gelatin mass ratios of 0.20 and 0.25 for three repeated experiments for each sample and their deviations are shown in Fig. 6. The magnitude of the force input was 270.2 ∓ 1.3 mN for the experiments in Fig. 6. It is seen that the experiments were repeatable for both samples (the average standard deviations were 0.022 and 0.008 mm for the phantoms with the 0.20 and 0.25 gelatin ratios, respectively). The results show that the steady-state displacement of the hemisphere decreases when the gelatin mass ratio increases from 0.20 to 0.25. As the shear modulus of the phantom increases with the increasing gelatin ratio, the hemisphere placed at the interface of the phantom with the gelatin ratio of 0.25 is expected to have smaller displacements. It is seen that the period of oscillations of the hemisphere placed at the sample interface decreases from 66.7 ms to 62.5 ms when the gelatin mass ratio increases from 0.20 to 0.25. Again, the period of oscillations of the hemisphere placed at the interface of the phantom with the gelatin mass ratio of 0.25 is expected to be lower due to the stiffness increase.

In conclusion, by matching the experimental and predicted steady-state displacements and the amplitudes of oscillations of the hemisphere placed at the interface of the

Fig. 6 The average of the experimentally identified responses of the hemisphere placed at the phantom interfaces with the gelatin mass ratios of 0.20 and 0.25 for three repeated experiments for each sample and their deviations (the magnitude of the force input is 270.2 ∓ 1.3 mN)
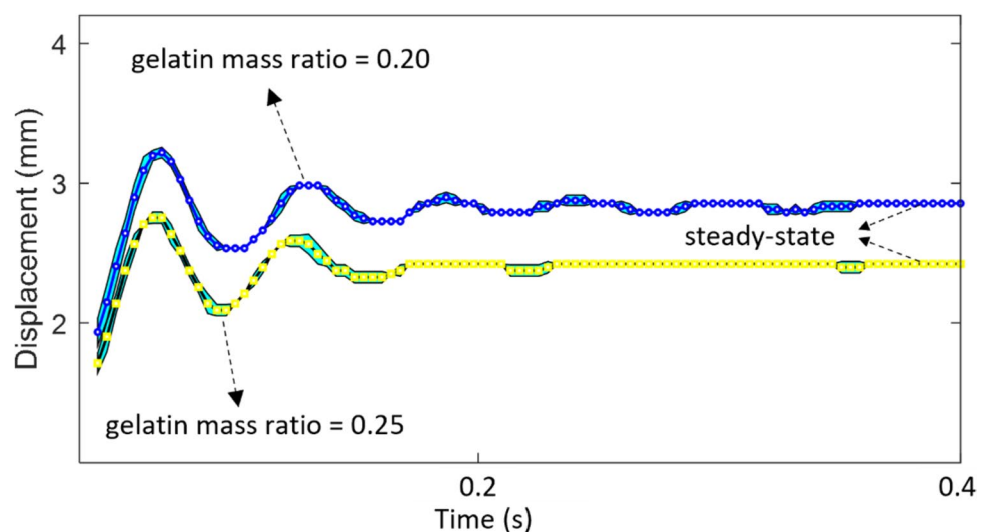
Fig. 7 The average of the experimentally identified and estimated response of the hemisphere placed at the interface of the phantoms with the gelatin mass ratios of 0.20 (left) and 0.25 (right) using the identified material properties
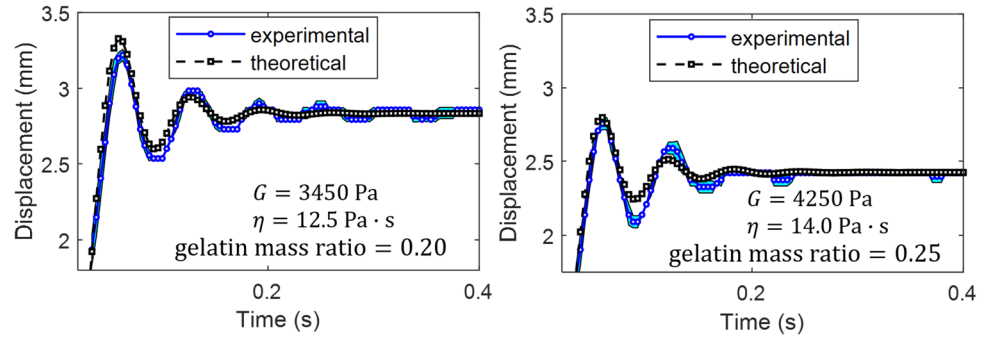

gelatin phantom as explained before, the shear modulus and viscosity of the phantoms with the gelatin mass ratios of 0.20 and 0.25 were determined. The shear modulus and viscosity of the phantom with the gelatin ratio of 0.20 were found to be to be $G = 3450$ Pa and $\eta = 12.5$ Pa·s, respectively. Similarly, the shear modulus and viscosity of the phantom with the gelatin ratio of 0.25 were identified to be to be $G = 4250$ Pa and $\eta = 14.0$ Pa·s, respectively. The experimental and estimated responses of the hemisphere placed at the interface of the phantoms with the gelatin mass ratios of 0.20 and 0.25 using the identified material properties are overlaid in Fig. 7. It is seen that the experimental and the theoretical results are quite similar. The results showed that the experimentally identified and theoretically predicted frequency of oscillations are almost the same.

The experimentally identified responses of the hemisphere placed at the interface of the phantom with the 0.25 gelatin ratio for two other force levels (i.e., 240.2 ∓ 0.4 and 291.5 ∓ 2.7 mN) are shown in Fig. 8. The experiments were highly repeatable, with average standard deviations of 0.015 and 0.029 mm for 240.2 ∓ 0.4 and 291.5 ∓ 2.7 mN, respectively (Fig. 8). By matching the experimental and theoretical steady-state displacements and the amplitudes of oscillations of the hemisphere placed at the interface of the gelatin phantom, the shear modulus and viscosity of the phantom were found to be to be $G = 4400$ Pa and $\eta = 14.0$ Pa·s when the force was 240.2 mN, and $G = 4150$ Pa and $\eta = 14.0$ Pa·s when the force was 291.5 mN. The estimated responses of the hemisphere placed at the interface of the phantom for these two force

levels using the identified material properties are included in Fig. 8. The results show that the amplitude of oscillations and the steady-state displacement of the hemisphere located at the phantom interface decrease with decreasing force amplitude, as expected. The shear modulus of the phantom for the force 240.2 - 291.5 mN was determined to be 4150-4400 Pa (the average being around 4300 Pa), while the viscosity was around 14.0 Pa·s. There was no significant change in the material properties for the soft gel for the force range covered here.

Overall, the identified material properties of the three phantoms with the gelatin mass ratios of 0.20, 0.25 and 0.29 are listed Table 2. The relaxation time (η/E) for each sample is included in Table 2. The material properties listed in Table 2 were identified using the averaged experimental responses of the sphere located at the phantom interface. However, as presented before, the deviations in the measured displacements of the hemisphere located at the phantom interface were quite small for the phantoms listed in Table 2 (i.e., the deviations in the measured displacements were less than 0.03 mm for all the phantoms). The frame rate of the camera was 240 fps, hence the deviation in the identified period of oscillation was around 2.2 ms. It is clear that the shear modulus and viscosity of the phantom increase as the gelatin mass ratio increases. As expected, the phantom becomes softer and less viscous as the gelatin mass ratio decreases. Similarly, the period of oscillations of the hemisphere placed at the phantom interface decreases (or its frequency of oscillations increases) as the gelatin mass

Fig. 8 Experimental and theoretical responses of the hemisphere placed at the interface of the phantom with the gelatin mass ratio of 0.25 exposed to 240.2 ∓ 0.4 mN (left) and 291.5 ∓ 2.7 mN (right)
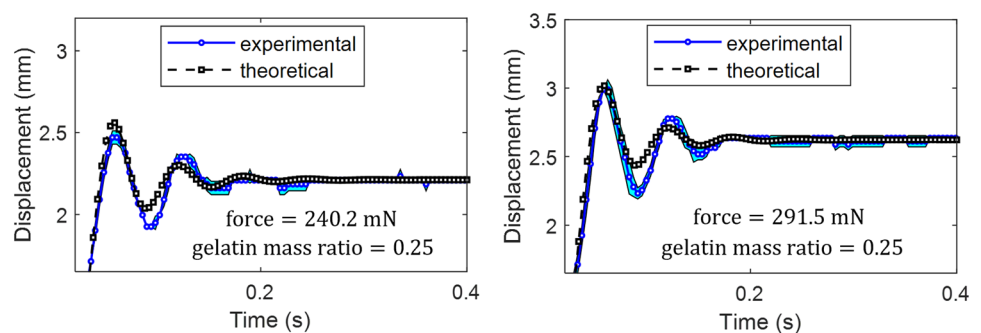
Table 2 Material properties of the three phantoms with the gelatin mass ratios of 0.20, 0.25 and 0.29 (the deviations in the measured force levels, displacements and periods of oscillations were less than 4 mN, 0.03 mm, and 2.2 ms, respectively)

Gelatin Mass Ratio	Force (mN)	Period of Oscillations (ms)	Shear Modulus (Pa)	Viscosity (Pa·s)	Relaxation Time (ms)
0.20 ($\rho = 1043.8$ kg/m^3)	270.2	66.7	3450	12.5	1.25
0.25 ($\rho = 1084.2$ kg/m^3)	240.2	66.7	4400	14.0	1.10
	270.2	62.5	4250	14.0	1.14
	291.5	62.5	4150	14.0	1.16
0.29 ($\rho = 1099.7$ kg/m^3)	265.7	58.3	4950	15.0	1.04

ratio increases due to stiffness increase when the external force is the same. For example, the period of oscillations of the hemisphere located at the phantom interface was 66.7, 62.5 and 58.3 ms for the phantoms with the 0.20, 0.25 and 0.29 gelatin ratios, respectively, when the force was around 270 mN. The period of oscillations decreases from 66.7 to 62.5 ms for the phantom with the 0.25 gelatin ratio when the force was increased from 240.2 to 291.5 mN. This is expected, because the stiffness of the system consisting of a spherical object located at the sample interface (hence, its natural frequency) increases with the increasing external load. There was no change in the period of oscillations when the force increased from 270.2 to 291.5 mN for the phantom with the 0.25 gelatin ratio. However, the uncertainty in the measured period of oscillation was 2.1 ms. The frame rate of the camera was not sufficient to capture this minute change in the period of oscillations.

After the response of the hemisphere placed at the interface of the phantom with the 0.29 gelatin ratio was measured, we cut a test sample with a cross-section of 25 mm x 25 mm (or $A = 6.25 \times 10^{-4}$ m^2) and a height of 30 mm (or $L = 0.03$ m) using the same sample. We then applied a force of around $F = 1.57$ N to this sample and we measured the amount of sample compression. It should be noted that it was not possible to detect the deformation of the sample as a function of time, and we could determine only the initial and final lengths of the sample under the applied load in this experiment. Overall, we determined that the sample was compressed by around 5.5 mm (or $\delta = 0.0055$ m) when a force of 1.57 N was applied to the sample. It is well known that the Young's modulus can be calculated using $E = \frac{FL}{A\delta}$ [48]. Based on these values, the Young's modulus of the sample was determined to be $E = 13700$ Pa. The shear modulus was calculated to be $G = \frac{E}{2(1+v)} = 4700$ Pa. It should be noted that the shear modulus was calculated to be 4950 Pa using the response of the hemisphere located at the same gelatin phantom (Table 2). It is seen that the difference is less than 5%.

The value of the shear modulus that matched the experimental and theoretical steady-state displacements of the hemisphere located at the sample interface was seen to simultaneously match the experimental and theoretical frequencies of oscillations. This further confirmed the validity of our method.

Using the expression for the shear wave speed, $v_s = \sqrt{G/\rho}$ [49], the time of reflection of the wave along the height (30 mm), width (100 mm) and length (170 mm) of the phantom was calculated to be around 28-33 ms, 94-111 ms and 160-188 ms, respectively. As seen in Table 2, the period of oscillations for the phantoms was around 58-67 ms in this study. The radiation damping due to shear waves for similar material properties and phantom dimensions was theoretically shown to be non-negligible using a non-viscous material [30] and a viscous material [31]. By including and ignoring the radiation damping in the analytical model, the responses of the hemisphere located at the interface of the phantom with the 0.25 gelatin ratio (force amplitude = 291.5 mN) were calculated. Oscillation amplitudes of the first three peaks were 3.12, 2.86, and 2.74 mm, when the radiation damping was ignored. The amplitudes of oscillations of the first three peaks were 3.02, 2.71, and 2.64 mm, when the radiation damping was included. The amplitudes of the first three peaks decreased by 3.2, 5.2 and 3.7%, respectively, when the radiation damping was included. Although the contribution of the radiation damping was not dominant, it was not negligible.

Before and after the experiment, we measured the constant force applied by some masses (e.g., 5 g), and the forces measured by the load cell were the same as the weights of these masses. In this work, we did not calibrate the load scale for dynamics forces. In future work, we aim to calibrate the setup with loads of known properties, to evaluate the effect of compliance and damping.

Based on a number of finite element analyses, the error for a ratio of the maximum displacement of the spherical object to the radius of the spherical object of 0.6 was shown to be less than 0.7% [30, 31]. It should be noted that the ratio of the maximum displacement of the spherical object to its radius is less than 0.3 in our study.

Although the experimental and theoretical results are quite similar, there are some discrepancies between them. The reasons for these discrepancies are evaluated here. In

the experiments, the electromagnetic force acts on the hemisphere after the sample is deformed by the weight of the hemisphere, while in the mathematical model it is assumed that the entire force is applied to the hemisphere simultaneously. This problem can be eliminated by revising the experimental setup or the mathematical model in the future. There may be some friction between the magnet and the hemisphere holder. Similarly, there may be an effect of friction between the hemisphere and phantom and the friction between the moving body and air. It should be noted that the mathematical model does not take into account these effects. In general, compared to other parameters such as elastic properties, the accurate modelling and experimentally identification of damping for all kind of materials is always challenging, because there are many factors that affect the damping of a system [5, 50–52].

The procedure proposed here for the characterization of the viscoelastic properties of soft materials is very versatile. As the frequency of oscillations of the spherical object placed at the sample interface depends on the mass and radius of the spherical object, experiments using spherical objects with different masses and/or radii can be performed to find the viscoelastic properties at different frequencies. The dependency of the viscoelastic properties of the soft material to the force level can be determined by just matching the experimentally identified and the theoretically predicted responses of the spherical object placed at the sample interface exposed to different forces. The spherical object and the test sample can be of any size, as long as an external force is applied to the sample and the response of the spherical object to the external force is measured. This means even the *in-situ* viscoelastic properties of structures can be measured using the method proposed in this manuscript. Furthermore, the spherical object can be pushed using any method such as ultrasonic and magnetic excitation and the response of the spherical object can be measured using various methods such as optical and ultrasonic imaging. In contrast to the atomic for microscopy [12] and indentation systems [17, 22], our method considers the inertia of the medium involved in motion and the radiation damping as well as the inertia of the spherical object located at the sample interface. Furthermore, the mathematical model used in our technique can simulate the change of the stiffness (hence, the change of the natural frequency) of the system consisting of a spherical object located at the sample interface with the altering external load, including the weight of the indenter and auxiliary parts. Compared to other methods in the literature [12, 21, 27], all these advantages of our method can provide a more accurate determination of material properties. On the other hand, our method needs to be revised to include various sources of friction. Overall, thanks to the simple experimental system and the comprehensive mathematical model that takes into account different system parameters including the shear modulus, density and viscosity of the soft sample, the mass and radius of the spherical object and the damping due to radiation, it is believed that the procedure used in this study would be used by many researchers for the identification of the viscoelastic properties of soft materials. The application of this method for the characterization of the viscoelastic properties of different tissues and tissue-mimicking materials and spheres with different masses and radii is considered as our future studies. In future work, we plan to use a high speed-camera with higher frame rate, achieve a finer image resolution and further reduce the effect of friction or alternatively take into account the effect of friction in the mathematical model. In addition to the Kelvin-Voigt model used in this study, we plan to evaluate different models (e.g., Maxwell model and standard linear solid model), and use different solution strategies in future work.

Conclusions

In this paper, a new approach for the identification of the viscoelastic properties of soft materials using the dynamic response of a spherical object placed at the sample interface was proposed. The spherical object placed at the sample interface was pressed using an electromagnet and the dynamic response of the spherical object was captured using a high-speed camera. The captured video was processed to identify the dynamic response of the spherical object. The dynamic response of the spherical object placed at the sample interface was estimated using a comprehensive analytical model. This model takes into account the shear modulus, viscosity, density and Poisson's ratio of the soft sample, the radius and density of the spherical object and the damping due to radiation. The shear modulus and viscosity of the soft sample were determined by matching the measured and predicted responses of the spherical object. The shear moduli of the phantoms with the gelatin mass ratios of 0.20, 0.25 and 0.29 were determined to be $G = 3450$, 4300 and 4950 Pa, respectively. The viscosities of the phantoms with the gelatin mass ratios of 0.20, 0.25 and 0.29 were identified to be $\eta = 12.5$, 14.0 and 15.0 Pa·s, respectively. The comparison of the experimentally identified and theoretically predicted frequency of oscillations further confirmed the identified material properties of the samples. The period of oscillations of the hemisphere placed at the phantom interface decreases (or its frequency of oscillations increases) and the shear modulus and viscosity of the phantom increase with the increasing gelatin mass ratio, as expected. Thanks to the uncomplicated experimental system and the comprehensive mathematical model that considers different system parameters including the shear modulus, density and viscosity of the medium, the mass and radius of the spherical object and the damping due to radiation, it is believed that the procedure used in

this study would be used by many researchers for the identification of the viscoelastic properties of soft materials in practical applications.

Appendix A: Summary of The Mathematical Model

The equation of motion of a spherical object located at an elastic interface was written as following in [30]:

$$f_e = f_i + f_s + f_r \tag{A1}$$

where f_e is the external force applied to the spherical object, f_i is the inertia force, f_s is the force related to the system stiffness, and f_r shows the component related to the damping of the oscillations of the spherical object due to the radiation of shear waves. A linear relationship between force (f_s) and displacement (u) was obtained by defining an equivalent stiffness coefficient or using the Taylor's expansion around the steady-state displacement as following [30]:

$$f_s \cong f(u_0) + \left.\frac{df}{du}\right|_{u_0}(u - u_0) = 1.5\frac{4E^*\sqrt{R}}{3}u_0^{1/2}u - 0.5\frac{4E^*\sqrt{R}}{3}u_0^{3/2} \tag{A2}$$

where the numerical value of the steady-state displacement can be calculated using $u_0 = \left(\frac{3f_0}{4E^*\sqrt{R}}\right)^{2/3}$. Here, the reduced Young's modulus for a homogeneous isotropic material is given by $E^* = 2G(1 + v)/(1 - v^2)$, where G and v are the shear modulus and Poisson's ratio of the medium material, respectively. By considering the external force as a rectangular pulse with the amplitude of f_0 and a duration of τ (i.e., the constant force f_0 is applied for a short time τ and then is removed), the equation of motion of the spherical object located at an elastic medium interface became as following [30]:

$$\frac{1}{3}\pi R^3\left(4\rho_s + \frac{u_0}{R}\rho\right)\ddot{u} + \frac{1}{2}\left(\beta + \frac{u_0}{R}\right)\left(\sqrt{\frac{\rho}{G}}R\right)\left(1 - \alpha\frac{u_0}{R}\right)$$
$$1.5f_0^{1/3}\left(\frac{4E^*\sqrt{R}}{3}\right)^{2/3}\dot{u} + \left(1 - \alpha\frac{u_0}{R}\right)1.5\left(\frac{4E^*\sqrt{R}}{3}\right)^{2/3}f_0^{1/3}u$$
$$= \left[1 + 0.5\left(1 - \alpha\frac{u_0}{R}\right)\right]f_0 \tag{A3}$$

where ρ and ρ_s are the densities of the medium material and spherical object, respectively, $\alpha = 0.1$, and $\beta = 0.5$. The analytical solution of equation (A3) was determined and given in equation (13) in [30]. This model was corrected for the Poisson's ratio of the medium of $v = 0.45$. Later, this mathematical model was updated in [31] to work for all practical Poisson's ratios (i.e., $v = 0.25 - 0.49$) of an elastic medium (no viscosity), given as following:

$$\frac{1}{3}\pi R^3\left(4\rho_s + \frac{u_0}{R}\rho\right)\ddot{u} + \frac{1}{2}\left(\beta + \frac{u_0}{R}\right)\left(\sqrt{\frac{\rho}{G}}R\right)$$
$$\left[1 - (v - 0.35)\frac{u_0}{R}\right]1.5f_0^{1/3}\left(\frac{4E^*\sqrt{R}}{3}\right)^{2/3}\dot{u}$$
$$+ \left[1 - (v - 0.35)\frac{u_0}{R}\right]1.5\left(\frac{4E^*\sqrt{R}}{3}\right)^{2/3}f_0^{1/3}u$$
$$= \left\{1 + 0.5\left[1 - (v - 0.35)\frac{u_0}{R}\right]\right\}f_0 \tag{A4}$$

The analytical solution for the dynamic response of the spherical object located at an elastic medium (no viscosity) interface (equation (A3) or (A4)) is straightforward. On the other hand, it is common in the literature to write the equation of motion in the frequency domain, include the viscosity effect in the frequency domain, and then solve the equation of motion using the inverse Fourier transform for systems containing viscoelastic media. This methodology has been widely used to calculate the dynamic response of a bubble or a non-deformable sphere placed inside a viscoelastic medium for the identification of the shear modulus and viscosity of tissues and tissue-mimicking materials [e.g., 1, 18, 20, 38–40]. Using this approach in the literature, the equation of motion for the spherical object located at an elastic medium interface in the time domain (i.e., equation (A4)) was first written in the frequency domain, and then the effect of the viscosity of the medium (η) was considered by replacing G with $G - j\omega\eta$ in [31]. Overall, the equation of motion for the spherical object located at a viscoelastic medium interface in the frequency domain was obtained as following [31]:

$$\frac{1}{3}\pi R^3\left(4\rho_s + \frac{u_0}{R}\rho\right)(-\omega^2 U) + \frac{1}{2}\left(\beta + \frac{u_0}{R}\right)\left(\sqrt{\frac{\rho}{G - j\omega\eta}}R\right)$$
$$\left[1 - (v - 0.35)\frac{u_0}{R}\right]1.5f_0^{1/3}\left(\frac{4\widetilde{E}^*\sqrt{R}}{3}\right)^{2/3}(-j\omega U)$$
$$+ \left[1 - (v - 0.35)\frac{u_0}{R}\right]1.5\left(\frac{4\widetilde{E}^*\sqrt{R}}{3}\right)^{2/3}f_0^{1/3}U$$
$$= \left\{1 + 0.5\left[1 - (v - 0.35)\frac{u_0}{R}\right]\right\}\left[-\frac{jf_0}{\omega}(e^{j\omega\tau} - 1)\right] \tag{A5}$$

where $\widetilde{E}^* = 2(G - j\omega\eta)(1 + v)/(1 - v^2)$, U is the Fourier transform of the displacement, ω represents the frequency, and $j = \sqrt{-1}$. The time-domain response of the spherical object located at a viscoelastic interface can be found by using the inverse Fourier transform which was given in equation (1) in the main text of this study. Interested readers may refer to [30, 31] for more details on the derivations of the mathematical models for a spherical object located at the interface of elastic and viscoelastic media.

Declarations

References

1. Urban MW, Nenadic IZ, Mitchell SA et al (2011) Generalized response of a sphere embedded in a viscoelastic medium excited by an ultrasonic radiation force. J Acoust Soc Am 130:1133–1141. https://doi.org/10.1121/1.3613939
2. Chim YH, Mason LM, Rath N et al (2018) A one-step procedure to probe the viscoelastic properties of cells by Atomic Force Microscopy. Sci Rep 8:14462. https://doi.org/10.1038/s41598-018-32704-8
3. Mijailovic AS, Qing B, Fortunato D, Van Vliet KJ (2018) Characterizing viscoelastic mechanical properties of highly compliant polymers and biological tissues using impact indentation. Acta Biomater 71:388–397. https://doi.org/10.1016/j.actbio.2018.02.017
4. Koruk H, Choi JJ (2019) Displacement of a bubble located at a fluid-viscoelastic medium interface. J Acoust Soc Am 145:EL410–EL416. https://doi.org/10.1121/1.5108678
5. Bezer JH, Koruk H, Rowlands CJ, Choi JJ (2020) Elastic deformation of soft tissue-mimicking materials using a single microbubble and acoustic radiation force. Ultrasound Med Biol 46:3327–3338. https://doi.org/10.1016/j.ultrasmedbio.2020.08.012
6. Qiang B, Greenleaf J, Oyen M, Zhang X (2011) Estimating material elasticity by spherical indentation load-relaxation tests on viscoelastic samples of finite thickness. IEEE Trans Ultrason Ferroelectr Freq Control 58:1418–1429
7. Nayar VT, Weiland JD, Nelson CS, Hodge AM (2012) Elastic and viscoelastic characterization of agar. J Mech Behav Biomed Mater 7:60–68. https://doi.org/10.1016/j.jmbbm.2011.05.027
8. Qian L, Zhao H (2018) Nanoindentation of soft biological materials. Micromachines (Basel) 9:654. https://doi.org/10.3390/mi9120654
9. Boots JNM, Fokkink R, van der Gucht J, Kodger TE (2019) Development of a multi-position indentation setup: Mapping soft and patternable heterogeneously crosslinked polymer networks. Review of Scientific Instruments 90:15108. https://doi.org/10.1063/1.5043628
10. Orikasa K, Bacca N, Agarwal A (2021) Meso/macro-scale ultra-soft materials' mechanical property evaluation device and testbed. Review of Scientific Instruments 92:73904. https://doi.org/10.1063/5.0046282
11. Helisaz H, Bacca M, Chiao M (2022) A New Characterization Procedure for Quasi-Linear Viscoelastic Materials Using Indentation Test: Validation with Finite Element and Experimental Results. Exp Mech 62:893–908. https://doi.org/10.1007/s11340-022-00837-7
12. Dakhil H, Gilbert DF, Malhotra D et al (2016) Measuring average rheological quantities of cell monolayers in the linear viscoelastic regime. Rheol Acta 55:527–536. https://doi.org/10.1007/s00397-016-0936-5
13. Peng B, Tang J, Wang P et al (2018) Rheological properties of cellulose nanocrystal-polymeric systems. Cellulose 25:3229–3240. https://doi.org/10.1007/s10570-018-1775-6
14. Ji Y, Dagro AM, Dorgant G et al (2022) A Comparison of Conventional Gel Stiffness Characterization Techniques with Cavitation Rheology. Exp Mech 62:799–812. https://doi.org/10.1007/s11340-022-00829-7
15. Puricelli L, Galluzzi M, Schulte C et al (2015) Nanomechanical and topographical imaging of living cells by atomic force microscopy with colloidal probes. Review of Scientific Instruments 86:33705. https://doi.org/10.1063/1.4915896
16. Garcia R (2020) Nanomechanical mapping of soft materials with the atomic force microscope: methods, theory and applications. Chem Soc Rev 49:5850–5884. https://doi.org/10.1039/D0CS00318B
17. Kontomaris S-V (2018) The Hertz Model in AFM Nanoindentation Experiments: Applications in Biological Samples and Biomaterials. Micro and Nanosystems 10:11–22
18. Cebrecos A, Jiménez N, Tarazona R et al (2021) Characterization of viscoelastic media combining ultrasound and magnetic-force induced vibrations on an embedded soft magnetic sphere. IEEE Trans Ultrason Ferroelectr Freq Control 68:3540–3548. https://doi.org/10.1109/TUFFC.2021.3097883
19. Levy BE, Oldenburg AL (2021) Single magnetic particle motion in magnetomotive ultrasound: An analytical model and experimental validation. IEEE Trans Ultrason Ferroelectr Freq Control 68:2635–2644. https://doi.org/10.1109/TUFFC.2021.3072867
20. Yoon S, Aglyamov SR, Karpiouk AB et al (2011) Estimation of mechanical properties of a viscoelastic medium using a laser-induced microbubble interrogated by an acoustic radiation force. J Acoust Soc Am 130:2241–2248. https://doi.org/10.1121/1.3628344
21. Boyer G, Laquièze L, Le Bot A et al (2009) Dynamic indentation on human skin in vivo: ageing effects. Skin Res Technol 15:55–67. https://doi.org/10.1111/j.1600-0846.2008.00324.x
22. Doss BL, Rahmani Eliato K, Lin K, Ros R (2019) Quantitative mechanical analysis of indentations on layered, soft elastic materials. Soft Matter 15:1776–1784. https://doi.org/10.1039/C8SM02121J
23. Huth S, Sindt S, Selhuber-Unkel C (2019) Automated analysis of soft hydrogel microindentation: Impact of various indentation parameters on the measurement of Young's modulus. PLoS One 14:e0220281
24. Moghaddam AO, Wei J, Kim J et al (2020) An indentation-based approach to determine the elastic constants of soft anisotropic

tissues. J Mech Behav Biomed Mater 103:103539. https://doi.org/10.1016/j.jmbbm.2019.103539

25. Kontomaris SV, Malamou A, Stylianou A (2020) A new approach for the AFM-based mechanical characterization of biological samples. Scanning 2020:2896792. https://doi.org/10.1155/2020/2896792

26. Vriend NM, Kren AP (2004) Determination of the viscoelastic properties of elastomeric materials by the dynamic indentation method. Polym Test 23:369–375. https://doi.org/10.1016/j.polymertesting.2003.10.006

27. Darling EM, Zauscher S, Guilak F (2006) Viscoelastic properties of zonal articular chondrocytes measured by atomic force microscopy. Osteoarthritis Cartilage 14:571–579. https://doi.org/10.1016/j.joca.2005.12.003

28. Koruk H (2021) Development of a model for predicting dynamic response of a sphere at viscoelastic interface: A dynamic Hertz model. IOP Conf Ser Mater Sci Eng 1150:012015. https://doi.org/10.1088/1757-899X/1150/1/012015

29. Koruk H (2021) Assessment of the models for predicting the responses of spherical objects in viscoelastic mediums and at viscoelastic interfaces. IOP Conf Ser Mater Sci Eng 1150:012016. https://doi.org/10.1088/1757-899X/1150/1/012016

30. Koruk H (2021) Modelling small and large displacements of a sphere on an elastic half-space exposed to a dynamic force. Eur J Phys 52:055006. https://doi.org/10.1088/1361-6404/ac0e42

31. Koruk H (2022) Development of an improved mathematical model for the dynamic response of a sphere located at a viscoelastic medium interface. Eur J Phys 43:25002. https://doi.org/10.1088/1361-6404/ac4647

32. Koruk H, Yurdaer SB, Koc HO, Besli A (2022) Identification of the viscoelastic properties of soft materials using a convenient dynamic indentation system and procedure. Mater Today Proc 57:464–468. https://doi.org/10.1016/j.matpr.2022.01.188

33. Koruk H, Besli A, Koc HO, Yurdaer SB (2022) Identification of material viscoelastic properties using the motion of a rigid sphere located at tissue-mimicking material interface in response to a dynamic force. Mater Sci Forum 73–78. https://doi.org/10.4028/p-oum2c1

34. Markidou A, Shih WY, Shih W-H (2005) Soft-materials elastic and shear moduli measurement using piezoelectric cantilevers. Review of Scientific Instruments 76:64302. https://doi.org/10.1063/1.1928407

35. Erpelding TN, Hollman KW, O'Donnell M (2005) Bubble-based acoustic radiation force elasticity imaging. Ultrasonics, Ferroelectrics, and Frequency Control, IEEE Transactions on 52:971–979. https://doi.org/10.1109/TUFFC.2005.1504019

36. Mikula E, Hollman K, Chai D et al (2014) Measurement of corneal elasticity with an acoustic radiation force elasticity microscope. Ultrasound Med Biol 40:1671–1679. https://doi.org/10.1016/j.ultrasmedbio.2013.11.009

37. Saharkhiz N, Koruk H, Choi JJ (2018) The effects of ultrasound parameters and microbubble concentration on acoustic particle palpation. J Acoust Soc Am 144:796–805. https://doi.org/10.1121/1.5050524

38. Ilinskii YA, Meegan GD, Zabolotskaya EA, Emelianov SY (2005) Gas bubble and solid sphere motion in elastic media in response to acoustic radiation force. J Acoust Soc Am 117:2338–2346. https://doi.org/10.1121/1.1863672

39. Aglyamov SR, Karpiouk AB, Ilinskii YA et al (2007) Motion of a solid sphere in a viscoelastic medium in response to applied acoustic radiation force: Theoretical analysis and experimental verification. J Acoust Soc Am 122:1927–1936. https://doi.org/10.1121/1.2774754

40. Karpiouk AB, Aglyamov SR, Ilinskii YA et al (2009) Assessment of shear modulus of tissue using ultrasound radiation force acting on a spherical acoustic inhomogeneity. IEEE Trans Ultrason Ferroelectr Freq Control 56:2380–2387

41. Kontomaris S-V, Malamou A (2020) Small oscillations of a rigid sphere on an elastic half space: a theoretical analysis. Eur J Phys 41:55004. https://doi.org/10.1088/1361-6404/ab9a0a

42. Aghahosseini A, Khosravifard A, Bui TQ (2019) Efficient analysis of dynamic fracture mechanics in various media by a novel meshfree approach. Theoretical and Applied Fracture Mechanics 99:161–176. https://doi.org/10.1016/j.tafmec.2018.12.002

43. Chandran PL, Barocas VH (2004) Microstructural mechanics of collagen gels in confined compression: Poroelasticity, viscoelasticity, and collapse. J Biomech Eng 126:152–166. https://doi.org/10.1115/1.1688774

44. Inman DJ (2013) Engineering Vibrations, Fourth Edi. Pearson Education, New Jersey

45. El Ghamrawy A, de Comtes F, Koruk H et al (2019) Acoustic Streaming in a Soft Tissue Microenvironment. Ultrasound Med Biol 45(1):208–217. https://doi.org/10.1016/j.ultrasmedbio.2018.08.026

46. Koruk H, Choi JJ (2018) Displacement of a bubble by acoustic radiation force into a fluid–tissue interface. J Acoust Soc Am 143:2535–2540. https://doi.org/10.1121/1.5034175

47. Maccabi A, Shin A, Namiri NK et al (2018) Quantitative characterization of viscoelastic behavior in tissue-mimicking phantoms and ex vivo animal tissues. PLoS One 13:e0191919

48. Weisbecker H, Unterberger MJ, Holzapfel GA (2015) Constitutive modelling of arteries considering fibre recruitment and three-dimensional fibre distribution. J R Soc Interface 12:20150111. https://doi.org/10.1098/rsif.2015.0111

49. Nowicki A, Dobruch-Sobczak K (2016) Introduction to ultrasound elastography. J Ultrason 16:113–124. https://doi.org/10.15557/JoU.2016.0013

50. Koruk H, Sanliturk KY (2012) Identification and removal of adverse effects of non-contact electromagnetic excitation in Oberst Beam Test Method. Mech Syst Signal Process 30:274–295. https://doi.org/10.1016/j.ymssp.2012.02.003

51. Sanliturk KY, Koruk H (2014) A new triangular composite shell element with damping capability. Compos Struct 118:322–327. https://doi.org/10.1016/j.compstruct.2014.07.053

52. Genc G, Koruk H (2017) Identification of the dynamic characteristics of luffa fiber reinforced bio-composite plates. Bioresources 12:5358–5368. https://doi.org/10.15376/biores.12.3.5358-5368